Clays and Clay Minerals, Vol. 41, No. 6, 668–679, 1993.

A CHEMICAL, XRD, AND ^{27}Al MAS NMR INVESTIGATION OF MIOCENE GULF COAST SHALES WITH APPLICATION TO UNDERSTANDING ILLITE/SMECTITE CRYSTAL-CHEMISTRY

PAUL A. SCHROEDER

Department of Geology, The University of Georgia, Athens, Georgia 30602

Abstract—This study assesses the distribution of Al and Fe in mixed-layer illite/smectites (I/S) in shales undergoing burial diagenetic changes, using evidence from ^{27}Al NMR, XRD, and chemical analyses. Samples studied include a sequence of mixed-layer I/S (ranging from 40% to 68% illite layers) in shales from a well located in the Caillou Island Oil Field, Terrebonne Parish, Louisiana, as well as synthetic mica-montmorillonite (Syn-1), Silver Hill illite (IMt-1), K-benonite (ISMt-1), an Fe-bearing muscovite, phengitic muscovite, and a randomly interstratified mixed-layer I/S with 50% illite layers. Using a simplified model, where Fe^{3+} isomorphously substitutes randomly for $^{[6]}$Al in the dioctahedral 2:1 structure, the ^{27}Al NMR signal intensities are examined with regard to the paramagnetic deshielding effect of the Fe^{3+}. The rapid decrease in paramagnetic deshielding with distance allows for a spherical "wipeout" model with a radius of 6 Å, over which there is complete effective paramagnetic line broadening (i.e., Al within the sphere is not "seen"). Using the average dimensions of a dioctahedral mica, the expected relative intensities of the octahedral and tetrahedral Al signal are determined as a function of Fe_2O_3 content.

Observed ^{27}Al signals, normalized per unit weight of Al_2O_3 and relative to the lowest Fe-bearing phase, show a clear trend of decreasing intensity with increasing Fe_2O_3 content. Normative fitting of oxide data to structural formulae reveals a similar trend of decreasing ^{27}Al intensity with increasing fraction of dioctahedral site occupied by Fe^{3+}. Agreement between the observed ^{27}Al intensities of low Fe-bearing 2:1 phyllosilicates and ^{27}Al intensities predicted using the wipeout model indicate regular ordering of Fe and Al within the low Fe-bearing phases. However, observed ^{27}Al intensities for the I/S specimens fall into a region where the amount of Al seen is in excess for the given X_{Fe}, thus indicating segregation of Al and Fe domains.

The second order quadrupole effect for the $^{[6]}$Al site in the I/S fraction of shales decreases very slightly with increasing depth and percent of illite in the I/S, but not enough to effect site quantitation. Quantitative apportionment of elements into the I/S phase of the <0.2 μm fraction using NMR constraints shows directly a trend of increasing number of $^{[4]}$Al sites and no change in the number of $^{[6]}$Al sites with increasing degree of illitization for samples from the Gulf Coast diagenetic environment. Stoichiometry indicates an approximate 1:1 substitution of tetrahedral Al for Si over the 40–68% range of illite in I/S examined.

Key Words—Burial diagenesis, Gulf Coast, Illite/smectite, Miocene, NMR.

INTRODUCTION

Al is the most common major metal cation that occupies both tetrahedral and octahedral sites in the sheets of natural 2:1 phyllosilicates. The technique of solid-state ^{27}Al magic-angle spinning (MAS) nuclear magnetic resonance (NMR) spectroscopy for identifying individual coordination sites is now common practice and has proven to be critically important for yielding accurate information about phyllosilicate crystal-chemistry (e.g., Kirkpatrick, 1988). Quantitative ^{27}Al NMR studies of octahedral aluminum ($^{[6]}$Al) and tetrahedral aluminum ($^{[4]}$Al) site populations within layer silicates have been a subject of debate (Goodman and Stucki, 1984; Sanz and Serratosa, 1984). However, more recent studies by Kinsey *et al.* (1985), Woessner (1989) and Morris *et al.* (1990) have demonstrated that, given proper experimental considerations, good agreement between NMR measurements of $^{[4]}$Al to $^{[6]}$Al ratios and the ratios calculated from structural formulae can be reached for many 2:1 phyllosilicates.

At the same time, the debate about the exact crystal-chemical structure of mixed-layer illite/smectites (I/S) in sediments undergoing changes during burial diagenesis continues to be open for additional constraints (Środoń *et al.*, 1986; Altaner *et al.*, 1988; Ahn and Buseck, 1990; and Schroeder, 1992a). Of the various paradigms that exist for the overall illitization reaction, two models are generally thought to account for the mechanisms responsible. The first model, known as the transformation model, requires the reaction to proceed via an *in situ* remodeling of smectite to illite. Concomitant with an increase in the proportion of illite layers in the I/S structure is a sequential collapse from randomly interstratified I/S to an ordered interstratified I/S to, finally, a long-range ordered interstratified I/S (Hower *et al.*, 1976; Bethke and Altaner, 1986; Moore and Reynolds, 1989). The second model is a dissolution-precipitation (diss/ppt) model, where smectite and possibly detrital illite dissolve to form

[1] ^{27}Al chemical shift frequency is reported in ppm units relative to the resonant Al frequency in a 1.0 M $AlCl_3$ solution.

authigenic illite. The diss/ppt model evolved from the views of Boles and Franks (1979) using chemical mass balance considerations and Pollastro (1985) using SEM-based mophology. Nadeau *et al.* (1984a–1984c) introduced the concept of discrete "fundamental" illite and smectite particles, which allowed the illitization process to be viewed as a crystal nucleation and growth phenomenon. Eberl and Środoń (1988), Inoue *et al.* (1988), and Lanson and Champion (1991) have since suggested Ostwald ripening as an additional mechanism involved in the diss/ppt of I/S.

Of all the mechanisms proposed for illitization, no single mechanism adequately describes the overall reaction. It is likely that several mechanisms operate simultaneously and that any given reaction pathway will be contingent upon specific geochemical conditions (i.e., time, temperature, initial smectite mineralogy, and associated mineralogy). For hydrothermal illitization, where illitization occurs on geologically small spatial scales and short temporal scales, there is strong evidence for both the transformation and diss/ppt mechanisms being involved (Eberl *et al.*, 1987; Inoue *et al.*, 1987; Eberl and Środoń, 1988; Whitney and Northrop, 1988). Identifying the appropriate reaction mechanisms involved in illitization during progressive burial in sedimentary basins is more difficult due to the complexity of local reactions involving feldspar diss/ppt (e.g., Milliken, 1989), organic matter maturation (e.g., Surdam and Crossey, 1987) and external reactions such as importing reactants (Howard, 1987). Despite these complexities, there remains a utility in using the crystal-chemical state of I/S as an indicator of the diagenetic history that sediments have experienced during progressive burial (Elliot *et al.*, 1991). The key for future attempts to employ I/S as an effective indicator (e.g., a geothermometer) lies with the prerequisite of accurate crystal-chemical characterization throughout the stages of the illitization.

The purpose of this paper is to employ the quantitative techniques of ^{27}Al MAS NMR, X-ray powder diffraction (XRD), and chemical analysis to characterize the changes in the structural chemistry of Al in diagenetic I/S from a sequence of sediments that have undergone progressive burial. Recent studies by Morris *et al.* (1990) have recognized an important effect of Fe on the ^{27}Al MAS NMR quantification $^{[4]}$Al and $^{[6]}$Al in montmorillonites. Because Fe concentration in I/S is typically seen to decrease with increasing degree of illitization (Hower *et al.*, 1976), this study also examines the significance of relationships between Fe_2O_3, $^{[4]}Al_2O_3$, $^{[6]}Al_2O_3$ and NMR signal intensity in I/S from a diagenetic sequence and other end-member 2:1 phyllosilicates used as references.

^{27}Al MAS NMR quantification

^{27}Al MAS NMR quantification of structural sites relies on the premise that all the ^{27}Al spin systems are equally detected and that the intensities are measurable in the final spectral output. Therefore, primary considerations are the factors that can affect the intensity and resolution of the spectra. In addition to the number of Al nuclei in the sample rotor of the MAS probe, line broadening (LB) mechanisms are the dominant factors that influence spectral quality. More precisely, LB can be attributed to: 1) dipolar interactions, 2) chemical shift anisotropies, 3) quadrupolar effects, and 4) paramagnetic components (Kirkpatrick, 1988). Finally, in the case where different Al coordinations are present (as is with the samples studied below), the extent of excitation of the quadrupolar-broadened spectrum may be a problem (Kirkpatrick *et al.*, 1986). The nature of each is discussed below to provide background and rationale for the NMR experiments conducted.

MAS alleviates the homogeneous LB problem due to dipolar interactions and chemical shift anisotropy and reduces the quadrupolar LB effect by a factor of about 3 to 4 (Behrens and Schnabel, 1982a). MAS also introduces the phenomenon of spinning side bands (SSB), which is related to the physical spinning of the sample. As the spinning frequency increases, SSB peaks both migrate in position away from the central peak and decrease in area (Kinsey *et al.*, 1985). Spinning frequencies now routinely operate in the region of 12 KHz, thus moving SSB $\pm$ 92 ppm[1] (at field strength of 11.74 T) outside the central peak position and well beyond the ~65 ppm distance that typically separates $^{[4]}$Al and $^{[6]}$Al sites in I/S. In contrast to the reciprocal relationship of decreasing SSB peak areas with increasing spin frequency, Kinsey *et al.* (1985) have also shown that, for many clay minerals, SSB peak areas increase with both increasing amounts of paramagnetic impurities and increasing primary field ($\mathbf{H}_0$). The relationship of increasing SSB intensity with increasing $\mathbf{H}_0$ has been clearly attributed to the presence of ferromagnetic impurities occurring as segregated domains (Oldfield *et al.*, 1983).

Debates about the quantitative validity of ^{27}Al MAS NMR center around the fact that ^{27}Al is a quadrupole nuclide (i.e., it has a nuclear spin (I) of 5/2). The nonzero electric field gradient at the Al site, expressed as the quadrupole coupling constant (QCC) and a nonspherical distribution of charge around the nucleus (an asymmetry parameter, η) combine to form a second order quadrupole effect (SOQE) (Behrens and Schnabel 1982b; Ganapathy *et al.*, 1982; Lippmaa *et al.*, 1986). The degree to which the SOQE modifies the chemical shift peak shapes is dependent on both the near neighbor environment of the Al and the experimental conditions.

Experimental pulse width effects on ^{27}Al quantification have recently been addressed by Kirkpatrick *et al.* (1986), who used both the theoretical analysis of Fenzke *et al.* (1984) and their own observations of free induction decay's (fid) from various aluminous glasses.

If only the central $\pm 1/2$ transition of a quadrupolar nuclide is excited, then the signal intensity dependence upon the QCC is negligible. This condition is met when the pulse width used for solids is $\leq 1/6$ the solution $\pi/2$ pulse time. Kirkpatrick *et al.* (1986) have shown by comparison of the signals per unit mass of Al in solids with solutions that, under the short-pulse-width conditions, nearly all the ^{27}Al signal is detectable in solids (with an estimated level of precision and accuracy of about 10%). More recently, Massiot *et al.* (1990), Alemany *et al.* (1991), and Taulelle *et al.* (1992) have presented a more formal protocol that allows for accurate quantification of noninteger quadrupole site populations, particularly for mineral phases bearing Al sites with drastically different QCCs and ηs. For reasons described below, this later protocol was not followed.

The magnitude of the SOQE can be assessed by examining the same sample at two different $\mathbf{H}_0$ values, because it is the only LB factor that decreases with increasing $\mathbf{H}_0$. As shown by Samoson (1985), the true chemical shift of a particular quantum transition is obscured by the complex electric field gradient interactions; however, the observed center of gravity for that same transition is modified by the field dependent quadrupole shift. The magnitude of the SOQE can be, therefore, assessed by use of an expression derived by Lippmaa *et al.* (1980), which uses the differences in the centers of gravitiy of ^{27}Al MAS NMR peaks at different field strengths.

Using this approach, Jakobsen *et al.* (1988), Woessner (1989), and Lindgreen *et al.* (1991) have assessed the QCC in a variety of smectitic and illitic clays. These studies found that the QCC ranges from 2 to 3 MHz for both $^{[4]}$Al and $^{[6]}$Al sites, with a tendency for slightly higher values in the $^{[4]}$Al site. These values are large enough to modify spectra; however, they are small when compared with other aluminosilicates (Ghose and Tsang, 1973; Lippmaa *et al.*, 1986). The magnitude and small range in QCC for both sites suggests peak shapes will exhibit equivalent responses, thereby assuring reasonable accuracy in site population quantification. For this reason, the protocol of Massiot *et al.*, (1990) was not employed.

A final aspect of ^{27}Al quantification regards the effect of paramagnetic LB due to the presence of Fe in the octahedral site. In a study of Fe-bearing clays, Morris *et al.* (1990) observed no clear relationship between LB and Fe^{3+} content, an observation also noted by Woessner (1989). However, Morris *et al.* (1990) did observe a relationship of greater signal loss with increasing Fe^{3+} content. The mechanism of homogeneous paramagnetic LB can cause substantial signal loss and, therefore, the possibility exists of Al sites not being detected. The presence of a signal will, therefore, depend upon the distance between Fe^{3+} and Al. If there is a nonuniform distribution of Fe^{3+}, then the paramagnetic LB effect will be minimized. Illitic clays contain more tetrahedral Al than montmorillonites; thus, the relationship between Fe^{3+} content and NMR signal intensity requires investigation of both $^{[4]}$Al and $^{[6]}$Al sites.

MATERIALS AND METHODS

Mineral specimens used in this study have been characterized in detail using XRD, electron microprobe, and far-infrared (IR) analyses (Schroeder, 1990, 1992a). Natural mixed-layer I/S from a well located in Caillou Island Oil Field, Terrebonne Parish, Louisiana, was studied as representative of materials from a burial diagenetic environment. The samples used were drill cuttings selected from Miocene shale intervals and were collected over the depth range of 1220 m to 5764 m. The reference minerals include the C.M.S. Repository reference materials Syn-1 (synthetic mica-montmorillonite), IMt-1 (Silver Hill illite), ISMt-1 (Mancos Shale), an Fe-bearing muscovite (East Morris, Connecticut), phengitic muscovite (Zacapa, Guatemala, American Museum of Natural History MVJ84-52-1), and a randomly ordered mixed layer I/S with 50% illite layers (I/S, I = 50, R = 0, Cameron, Arizona). All clay samples were pretreated for removal of labile organics, carbonates, and both iron oxide and hydroxide coatings (Schroeder, 1992a). Samples were then sized to the <0.2 μm fraction. XRD analysis of the I/S in the shales indicates a range in ordering of I/S layer types from R = 0 to R = 0.5 and a range of 40% to 68% 10 Å (illite-type) layers in the mixed-layer structure.

All samples were analyzed by MAS NMR at 7.05 T (78.39 MHz) using a home built spectrometer housed at the Yale Department of Chemistry. The spectrometer was equipped with a Doty Scientific 5 mm high-speed spinning probe (10–12 KHz), using a Si_3N_4 rotor capable of holding approximately 100 mg of sample. Pulse programing and data acquisition were performed using a TECMAG/MacNMR interface, controlled by a Macintosh II computer. Realizing that there was the potential for the octahedral and tetrahedral Al sites to have different selectivities, experiments were conducted using variable input voltages and pulse lengths. In this way, nutation differences (i.e., the apparent $\pi/2$ times) between the two sites could be assessed. Spectra were collected using a two-phase cycle pulse sequence. Based on the nutation studies, experimental parameters were optimized for quantification of both Al sites and included an input power of 0.55 V (peak-to-peak), a recycle delay of 2 s and a pulse length of 2 μs (1/6 of a solution $\pi/2$ pulse). Each sample was scanned 200 times into a fid of 1024 data points and zero-filled to 2048 data points. Each fid was left-shifted one data point (20 μs) to eliminate the effect of pulse break through and then multiplied by 150 Hz or LB before being Fourier-transformed. The particular MAS probe used in this study contained a significant background resulting from Al in the variable tuning capacitors.

Each sample spectrum had this background (collected from a blank experiment under the exact same conditions) subtracted after processing of the signal. Peak areas (including sideband contributions) were determined by cutting and weighing using a linear background fit. Intensity measurements were normalized by the sample weight in the rotor for each experiment. Left-shifting of the data unfortunately compromises quantitative accuracy because of the difficulties in phasing of the spinning side bands. The error in accuracy $^{[4]}$Al and $^{[6]}$Al site quantification may be as much as 10%. Repeated measurement of the same sample yielded an intrumental precision that average about ±5% of the aluminum oxide values reported for each site type.

Five selected I/S samples were analyzed at 11.74 T (130.24 MHz) using a Fourier-transform NMR spectrometer housed at the University of Illinois at Urbana. The spectrometer was equipped with a Doty Scientific 5 mm high-speed spinning probe and Nicolet 1280 data system (R. J. Kirkpatrick, personal communication). Spectra were collected using a Bloch decay experiment, with a recycle delay of 600 ms and a pulse length of 1.4 μs (1/6 of a solution $\pi/2$ pulse). Each sample was scanned 1000 times into a fid of 2048 data points, zero-filled to 4096 data points, and multiplied by 100 Hz of LB before being Fourier-transformed into the final output. Peak areas were determined with the same procedure used at 7.05 T.

Quantitfication of I/S chemistry

The very fine grained nature of detrital and diagenetic clays common in most shales makes their separation via centrifugation or magnetic methods impossible (Tellier *et al.*, 1988). Consequently, quantitative clay mineralogy of the <0.2 μm fraction is required. The procedure for quantitative phase analysis utilizes full pattern XRD and calculated mineral intensity factors (Schroeder, 1992a). Accuracy of the XRD estimates of mineral weight percentages is about ±10% of the values reported. Precision is about ±3%.

In order to acertain the chemistry of the I/S phase in the fine fraction the following general mixing equation was used,

$$Me_xO_{y\ I/S} = \frac{Me_xO_{y\ TOTAL} - W_I Me_xO_{yI} - W_K Me_xO_{y\ K}}{W_{I/S}} \quad (1)$$

where $Me_xO_{y\ TOTAL}$ is the total weight fraction of an oxide (e.g., Al_2O_3) in the mixture and W equals the weight fractions of the phases illite (I), illite/smectite (I/S), and kaolinite (K). The data used for this study can be found in Tables 1 and 2 of Schroeder (1992a).

The stoichiometry of the discrete kaolinite and illite could not be independently measured; therefore, the following assumptions were made. Oxide weight fractions for kaolinite were reasonably assumed to be: $Al_2O_{3_K} = 0.3749$, $SiO_{2_K} = 0.4640$, $Fe_2O_{3_K} = 0.0009$, and 0.0000 for all other oxides (Giese, 1988). The assumed values for discrete illite are more tenuous because of the broad range of isomorphous substitution seen in illites (see e.g., Newman and Brown, 1987, Table 1.22). The stoichiometry of illite for input into Eq. (1) was assessed with two different approaches. First, an average of published values for end-member illites was used (Newman and Brown, 1987). Secondly, values were derived by extrapolating to the 1.0 weight fraction intercept in plots of weight fraction illite *vs.* weight fraction oxide using samples from this study. Surprisingly, both approaches gave about the same values. Final oxide weight fractions used for discrete illite were: $Al_2O_{3_I} = 0.2053$, $SiO_{2_I} = 0.5739$, $Fe_2O_{3_I} = 0.0894$, $K_2O_I = 0.0800$, $Na_2O_I = 0.0000$, and $MgO_I = 0.0464$.

Results from the ^{27}Al NMR peak area measurements allowed for further quantification of tetrahedral and octahedral site occupancies in the samples. The distribution of Al in the I/S portion of the sample was obtained with the following relationships. Given the total Al_2O_3 content of the mixture:

$$Al_2O_{3_{TOTAL}} = W_I Al_2O_{3_I} Al_I^4 + W_I Al_2O_{3_I} Al_I^6 + W_K Al_2O_{3_K} Al_K^6 + W_{I/S} Al_2O_{3_{I/S}} Al_{I/S}^4 + W_{I/S} Al_2O_{3_{I/S}} Al_{I/S}^6 \quad (2)$$

and the ratio of $^{[4]}$Al to $^{[4]}$Al + $^{[6]}$Al:

$$\frac{Al_{TOTAL}^4}{Al_{TOTAL}^4 + Al_{TOTAL}^6} = \frac{W_I Al_2O_{3_I} Al_I^4 + W_{I/S} Al_2O_{3_{I/S}} Al_{I/S}^4}{Al_2O_{3_{TOTAL}}} \quad (3)$$

it is possible to rearrange and solve simultaneously for the $^{[4]}Al_2O_3$ and $^{[6]}Al_2O_3$ content of the I/S:

$$W_{I/S} Al_2O_{3_{I/S}} Al_{I/S}^4 = \left(Al_2O_{3_{TOTAL}} \frac{Al_{TOTAL}^4}{Al_{TOTAL}^4 + Al_{TOTAL}^6} \right) - W_I Al_2O_{3_I} Al_I^4 \quad (4)$$

and

$$W_{I/S} Al_2O_{3_{I/S}} Al_{I/S}^6 = Al_2O_{3_{TOTAL}} - W_I Al_2O_{3_I} Al_I^4 - W_I Al_2O_{3_I} Al_I^6 - W_K Al_2O_{3_K} Al_K^6 - W_{I/S} Al_2O_{3_{I/S}} Al_{I/S}^4 \quad (5)$$

Assumed weight fractions of Al_2O_3 distributed into tetrahedral and octahedral sites for illite (I) and kaolinite (K) phases were $Al_I^4 = 0.198$, $Al_I^6 = 0.812$, and $Al_K^6 = 1.000$, respectively.

METHODOLOGY

The principal goal of this work is to use the quantitative capability of ^{27}Al MAS NMR in conjunction

https://doi.org/10.1346/CCMN.1993.0410605 Published online by Cambridge University Press

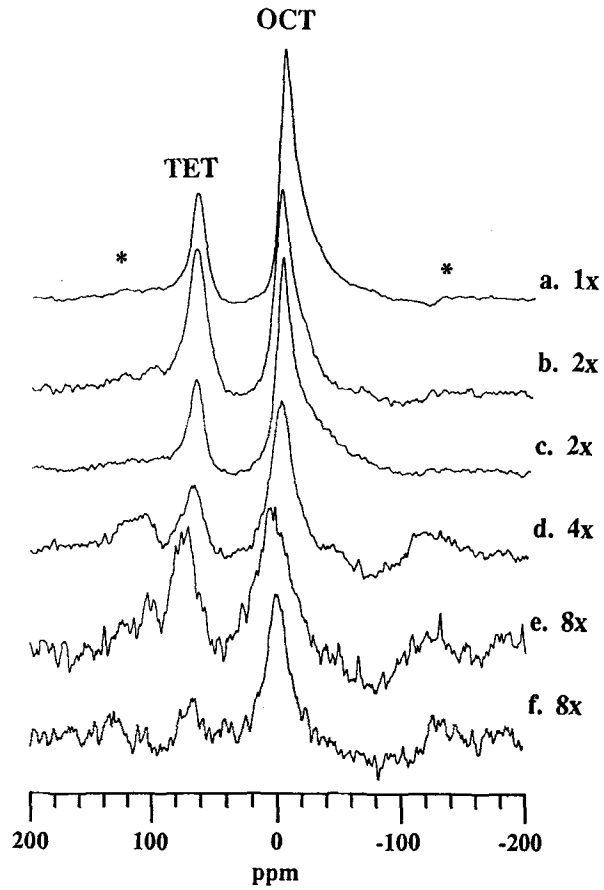

Figure 1. ^{27}Al NMR spectra of reference materials at 7.05 T: a) Syn-1 (synthetic mica-montmorillonite); b) phengitic muscovite; c) ISMt-1, K-bentonite, Mancos shale (I = 65%, R = 0); d) IMt-1 (illite, Silver Hill, Mont.); e) Fe-bearing muscovite (East Morris, Connecticut; and f) mixed-layer I/S, Cameron, Arizona, Yale Peabody Museum #002M-DS1 (I = 50%, R = 0). All spectra were collected and processed using identical experimental conditions (see text). The vertical scaling factor, relative to Syn-1, is noted to the right of each spectrum. OCT and TET denote central transition peak for octahedral and tetrahedral sites, respectively. Asterisks (*) denote octahedral spinning side bands.

with XRD and chemical analysis to identify the crystal-chemical changes of the I/S phases in Gulf Coast shales. Prior to the direct application of NMR results to the problem of I/S phase characterization, there first must be an assessment of methodology. In other words, an assessment of potential factors that can affect the measured peak areas and cause inaccuracy in the estimate of Al site populations. Subsequently, the results section examines the magnitude of the SOQE for [4]Al and [6]Al sites in I/S from the Gulf Coast shales and the discussion uses the various quantitative techniques to constrain the chemistry of I/S and explores the implications of these results for the mechanisms by which illitization in Gulf Coast shales proceeds.

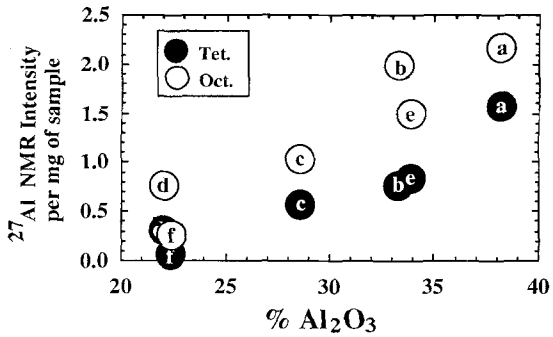

Figure 2. A plot of reference material Al_2O_3 content *vs.* the [6]Al and [4]Al NMR signal intensities (normalized per mg of sample). Sample identifications same as in Figure 1.

Iron effects on ^{27}Al intensity measurements

^{27}Al NMR spectra for the reference K-micas and illitic clays at 7.1 T are shown in Figure 1. Spectra have been arranged by relative signal-to-noise, each scaled with respect to Syn-1. As discussed previously, given the proper and constant experimental conditions, the integrated intensity is a function of the number of Al nuclei present in the rotor and LB mechanisms that can attenuate the signal. Figure 2 is a plot of Al_2O_3 content of the reference materials *vs.* both [4]Al and [6]Al NMR signal intensities (normalized per mg of sample). The expected positive trend is revealed. Isomorphous substitution of Fe^{3+} for Al^{3+} into octahedral sites of illitic clays also manifests a negative relationship between Fe_2O_3 and Al_2O_3 content (not shown). The interdependence of Fe_2O_3 and Al_2O_3 content, therefore, leads to a covariance between the intensity of [6]Al signal and Fe_2O_3 content, which is seen in Figure 3. Interestingly, there is also a dependence of the [4]Al signal on Fe_2O_3 content, although Fe^{3+} predominantly occupies octahedral sites. The following questions remain: 1) What is the magnitude of signal loss for the [6]Al and [4]Al sites resulting from paramagnetic LB due to the presence of Fe^{3+}; and 2) what does the

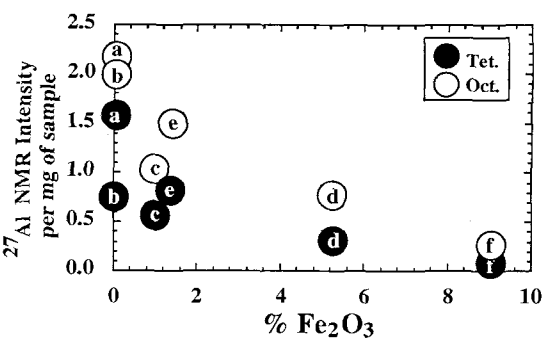

Figure 3. A plot of reference material Fe_2O_3 content *vs.* the [6]Al and [4]Al NMR signal intensities. Sample identifications same as in Figure 1.

https://doi.org/10.1346/CCMN.1993.0410605 Published online by Cambridge University Press

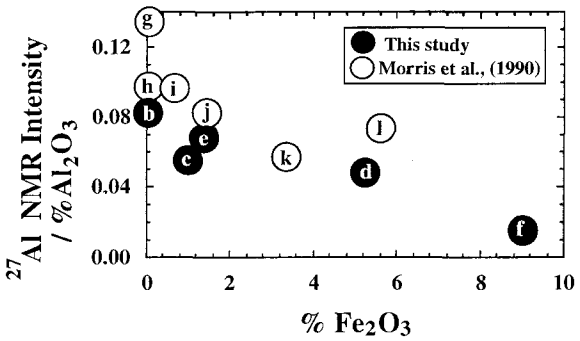

Figure 4. Ratio of the total normalized ^{27}Al NMR signal intensity to Al_2O_3 *vs.* Fe_2O_3 content. Data points with open circles are from Morris *et al.* (1990) and include g = kaolinite; h = Barasym (synthetic mica-montmorillonite); i = STx-1, Ca-montmorillonite, Gonzales County, Texas; j = SAz-1, Ca-montmorillonite, Cheto, Arizona; k = SWy-1, Na-montmorillonite, Crook County, Wyoming; and l = Amory montmorillonite, Amory, Massachusetts.

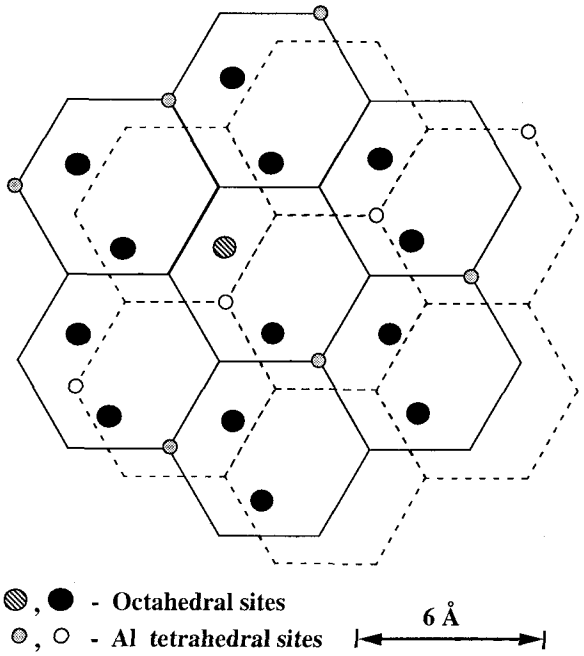

Figure 5. Dioctahedral 2:1 layer structure (view perpendicular to *ab* plane) showing the locations of dioctahedral metal center site (striped circle), coplaner dioctahedral sites (black circles), tetrahedral silica network (solid and dashed lines are top and lower planes, respectively), and $^{[4]}$Al substitution sites with an assumed Si:Al of 3:1 and regular ordering (small stippled and open circles).

relationship between Al signal strength and Fe_2O_3 content imply about the ordering of Fe^{3+} in the octahedral sheet?

To assess the Fe^{3+} effect on the NMR signal, total integrated NMR intensity (normalized by Al_2O_3 content of the sample) is plotted *vs.* Fe_2O_3 in Figure 4. A trend of about a 10% signal loss for each 1% increase in Fe_2O_3 is seen. Complete signal loss occurs at about 11% Fe_2O_3. For comparative purposes, the NMR intensity measurements at 9.40 T by Morris *et al.* (1990) have been rescaled through normalization to the sample Syn-1, a specimen examined in both studies. It is not clear if the intensities reported by Morris *et al.* (1990) were normalized per mg of sample or if the exact same sample weight was used in all experiments; surprisingly, however, when the Al_2O_3-normalized intensities are plotted *vs.* Fe_2O_3 content (Figure 4), they corroborate the relationship of about a 10% signal loss with each 1% increase in Fe_2O_3. This agreement of results suggests that the LB signal loss effect, due to paramagnetic Fe^{3+} substitution for $^{[6]}$Al, is similar in both montmorillonitic and illitic clays.

The relationship between Fe^{3+} content and total Al NMR signal intensity provides further insight into the ordering of Fe^{3+} in illitic clays. The following analysis assumes a simplified model, where Fe^{3+} isomorphously substitutes, on a regular ordered basis, for $^{[6]}$Al. The paramagnetic deshielding effect due to unpaired electrons in a neighboring atom is proportional to $1/r^3$, where r is the expected distance of an electron from the nucleus (Kirkpatrick, 1988). Because of this rapid decrease with distance, it is reasonable to assume a spherically modelled system, over which there is a radius of complete effective paramagnetic LB. Beyond this "wipeout" distance, there is very little effect. Morris *et al.* (1990) have recently demonstrated that for Fe centers in 2:1 clay structures, a distance of about 6 Å is the average maximum distance for complete paramagnetic LB loss of the Al signal.

Further assuming that the Al_2O_3-normalized NMR intensities of the lowest Fe content samples have the maximum measurable intensities (i.e., all the Al is "seen") and the Fe is evenly distributed, then the amount of signal loss is determined by the abundance of Fe relative to the number of Al atoms in octahedral and tetrahedral sites that lie within the wipeout sphere. Figure 5 depicts an idealized dioctahedral 2:1 structure that can be used as a visual aid to assess interatomic distances from an Fe^{3+} centered site to nearby tetrahedral and octahedral sites. Using lattice parameters typical of a dioctahedral mica (a = 5.2 Å, b = 9.0 Å, c = 10.0 Å) in an octahedral plane, there are a total of twelve neighboring dioctahedral sites within a 6 Å radius of metal centered site: Three nearest neighbors (NN) occur at a distance of about 3.0 Å, and nine second-NN sites at a distance of about 5.3 Å. The expected relative intensity of an $^{[6]}$Al signal under this condition is, therefore, related to the total number of dioctahedral sites within the sphere ($n_{[6]}$) and the probability that those octahedral sites are not occupied by Fe^{3+}. Using a mean field approximation, this relative intensity ($I_{^{[6]}Al}$) can be expressed as:

https://doi.org/10.1346/CCMN.1993.0410605 Published online by Cambridge University Press

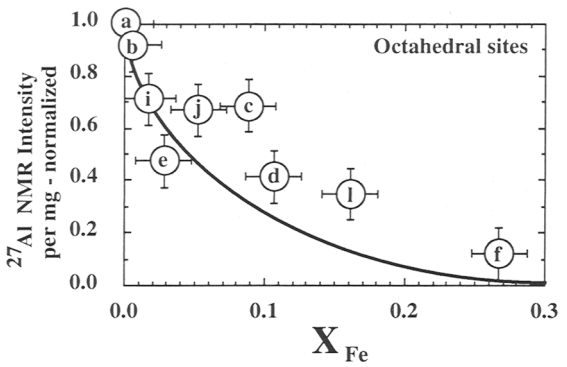

Figure 6. Normalized observed intensities of octahedral peaks *vs.* fraction of Fe occupying dioctahedral sites (X_{Fe}). Error bars represent experimental reproducibility of measurements (approximately σ_{sd}). The line on the plot represents expected intensities, assuming an idealized random distribution of Fe^{3+} in dioctahedral sites and a 6 Å sphere of effective paramagnetic LB that includes 12 neighboring Al^{3+} dioctahedral sites. See Figures 1 and 4 for sample identifications.

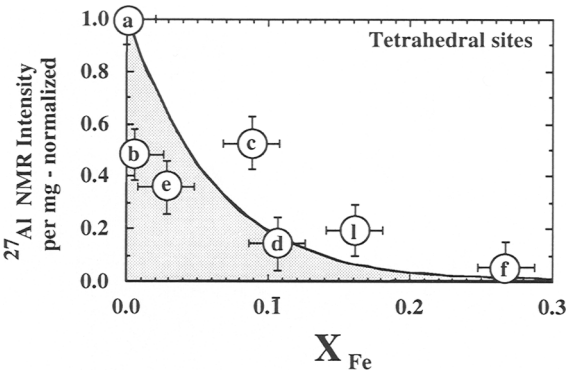

Figure 7. Normalized observed intensities of tetrahedral peaks *vs.* fraction of Fe occupying dioctahedral sites (X_{Fe}). The line on the plot represents expected [4]Al intensities, assuming an idealized random distribution of Fe^{3+} in dioctahedral sites and a 6 Å sphere of effective paramagnetic LB that includes 16 neighboring tetrahedral sites. The probabilities of [4]Al detection due to occupancy of the [4]Si site would fall below the curve. See Figures 1 and 4 for sample identifications.

$$I_{[6]Al} = (1 - X_{Fe})^{n[6]} \quad (6)$$

In this example, where $n_{[6]} = 13$ (including the centered site) and X_{Fe} = the fraction of dioctahedral sites occupied by Fe^{3+}, the point of signal loss occurs quite rapidly as shown in Figure 6.

At the same time, a total of sixteen tetrahedral sites occur within a 6 Å radius of a dioctahedral metal centered site; four NN tetrahedral sites at about a distance of 3.3 Å; four second-NN and eight third-NN at distances of about 4.4 Å and 5.5 Å, respectively. In this case, the number of detectable [4]Al atoms is additionally dependent on the fraction of [4]Al substituted into [4]Si sites. For example, in muscovite, there is one [4]Al substitution per half unit cell and nearly a regular ordering of [4]Al (Herrero, 1985; Herrero *et al.*, 1985a; Herrero *et al.*, 1985b; Herrero *et al.*, 1987). Under these idealized conditions, the expected relative intensity of an [4]Al signal is then related to X_{Fe}, the total number of tetrahedral sites ($n_{[4]}$) and the amount of [4]Al substitution for [4]Si. Again, using a mean field approximation, this realtive intensity ($I_{[4]Al}$) can be expressed as:

$$I_{[4]Al} = \left(\frac{[4]Al}{[4]Al + [4]Si}\right)(1 - X_{Fe})^{n[4]} \quad (7)$$

In this example, where $n_{[4]} = 16$, signal loss also occurs quite rapidly and is shown in Figure 7.

Figures 6 and 7 contain the normalized observed intensities for the octahedral and tetrahedral sites, respectively. The phengitic muscovite and Syn-1, containing the lowest amount of Fe^{3+}, exhibit the most intense signal per unit weight of Al_2O_3. In other words, all the Al is "seen" by an NMR experiment. The lines plotted on Figure 6 and 7 are the expected relative intensities of [6]Al and [4]Al signals, given by Eqs. (6) and (7) using the idealized conditions. The observed values for the relatively low Fe-bearing true micas reasonably fall in the same region as lines predicting regular ordering of Fe and Al. The illitic specimens clearly fall into the region where the amount of Al seen is in excess for the given amount of Fe. This is evidence for the distribution of Fe into segregated domains. The fact that ^{27}Al signals are still observable in higher Fe content samples indicates that either the 6 Å value cited by Morris *et al.* (1990) is too large or that there is a nonuniform distribution of Fe^{3+} within the structures. No independent tests have been conducted to determine whether the Fe^{3+} resides entirely in the octahedral sheet or if other Fe-bearing compounds remain as residual impurities. All samples were pretreated for the removal of Fe-oxide and hydroxide coatings. Therefore, for the purpose of this study, it is assumed that Fe impurity effects have been minimized.

The issue remains as to whether or not the Fe^{3+} signal loss affects the [4]Al and [6]Al sites equally. Trends in signal loss per fraction of Fe for both [4]Al and [6]Al sites are roughly equivalent. These results indicate that for the samples studied, paramagnetic LB from the presence of Fe^{3+} acts equally on both [4]Al and [6]Al sites, although the data quality limits this conclusion.

RESULTS

SOQE of I/S in Gulf Coast shales

^{27}Al NMR spectra for selected Gulf Coast shale intervals at field strengths of 7.05 T and 11.74 T are shown in Figures 8 and 9, respectively. The low field spectra appear noisier than the high field spectra, primarily because fewer scans were collected (200 *vs.* 1000) and because the 7.05 T background subtraction process

https://doi.org/10.1346/CCMN.1993.0410605 Published online by Cambridge University Press

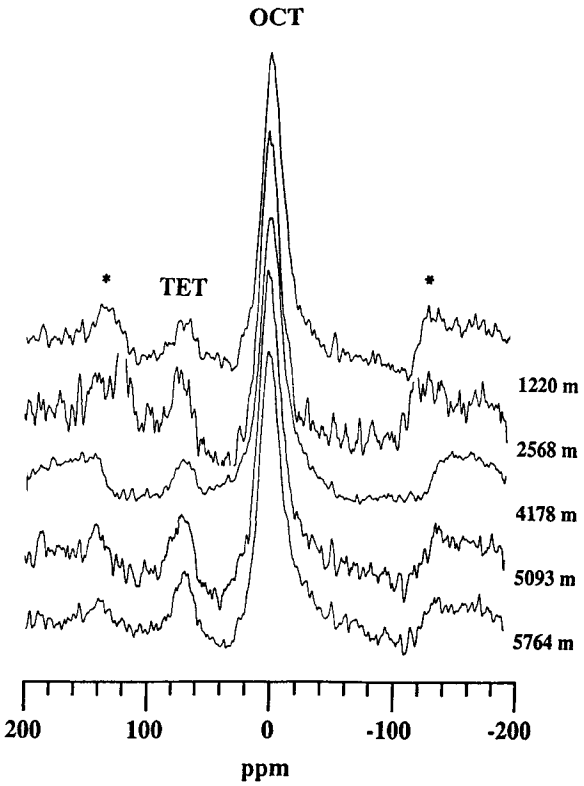

Figure 8. Background corrected ^{27}Al NMR spectra of <0.2 μm fraction of Gulf Coast shales at 7.05 T. See text for experimental conditions. OCT and TET denote central transition peak for octahedral and tetrahedral sites, respectively. Asterisks (*) denote octahedral spinning side bands.

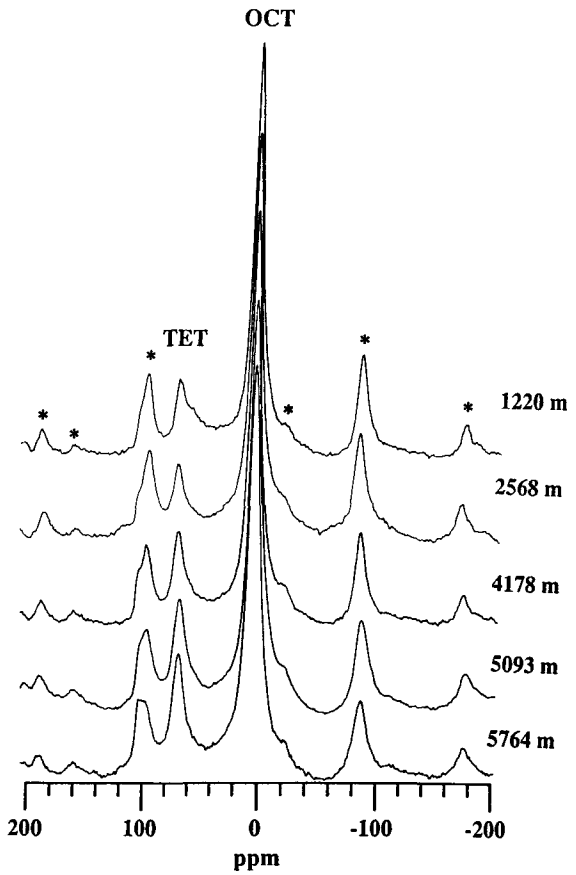

Figure 9. ^{27}Al NMR spectra of <0.2 μm fraction of Gulf Coast shales at 11.74 T. See text for experimental conditions. Asterisks (*) denote octahedral and tetrahedral spinning side bands.

has amplified background noise by a factor of two. The high spinning speeds have virtually eliminated the peak overlap problem at both fields. The observed tetrahedral and octahedral peak maxima (δ_p) at the two field strengths are reported in Table 1, with an experimental error of $\pm$ 1 ppm.

The peak shapes are very similar to those of other natural illitic clays (Jakobsen *et al.*, 1988; Woessner, 1989; Lindgreen *et al.*, 1991), showing a generally Gaussian line shape. The low field spectra exhibit an asymmetry to the low energy side of δ_p. As discussed previously, Woessner (1989) and Lindgreen *et al.* (1991), using the technique of Samoson (1985) and Lippmaa *et al.* (1986), have demonstrated QCC values range from 2 to 3 MHz for [4]Al and [6]Al sites in illitic clays. Theoretically, the ratio of line widths at the field strengths of 7.1 and 11.4 T, in Hz, is 1.7 (using Eqs. (2) and (3) from Lippmaa *et al.*, 1986). The observed line width ratios in this study average about 2.2 and 2.4 in ppm or 1.3 and 1.4 in Hz for the [4]Al and [6]Al sites, respectively (Table 1). The observed line width ratios, therefore, indicate that the primary cause of LB can be attributed to the SOQE.

Spectra at both field strengths show a small increase in LB with increasing degree of illitization for both Al sites, an exception being the deepest low field [4]Al peak (Table 1). These trends, although slight, indicate that the average local environment of both Al sites is changing with depth as a result of some LB factor. Recalling that the SOQE is the only field dependent LB factor and ratioing of the line widths at two field strengths should "flush" all other LB trends. From Table 1, it can be seen that the ratio of the [6]Al line widths exhibit a small but perceptible decrease with increasing depth. This trend, although subtle, suggests that LB from the SOQE decreases very slightly with depth and that the overall trend of increasing LB must be attributed to some other LB effect.

A possible candidate for the cause of increased LB with depth could be paramagnetic effects. The trend of decreasing Fe_2O_3 content in the I/S with the increasing degree of illitization (Table 2) appears to contradict this proposition of an increased paramagnetic LB effect with depth. However, as the sediments experience higher temperatures and longer burial history, it may

https://doi.org/10.1346/CCMN.1993.0410605 Published online by Cambridge University Press

Table 1. ^{27}Al chemical shift peak maxima (δ_p) and full width at half maximum (FWHM) at 7.05 T and 11.74 T for the <0.2 μm fraction from selected shale intervals.

Depth (m)	δ_p (ppm) at 7.05 T	FWHM (ppm)	δ_p (ppm) at 11.74 T	FWHM (ppm)	Ratio of FWHM 7.05 T to 11.74 T
		Tetrahedral Al sites			
1220	69	18	70	8.5	2.1
2568	69	19	70	8.5	2.2
4178	69	21	70	9.4	2.2
5093	68	23	70	9.4	2.4
5764	68	19	70	10.3	1.8
		Octahedral Al sites			
1220	3	21.7	4	8.3	2.6
2568	3	21.7	4	8.6	2.5
4178	3	22.0	4	9.3	2.4
5093	3	22.9	4	10.5	2.2
5764	3	24.1	4	10.5	2.3

be that Fe^{3+}, in the form of hydroxides and oxy-hydroxides, dehydroxylate to form stable Fe-oxides (Taylor, 1980). These forms are inclined to be more resistant to the citrate-dithionate-bicarbonate treatment for removal of the Fe-phases. The presence of the antiferromagnetic oxide, hematite, has been shown to produce little effect on side band intensity of ^{27}Al MAS NMR spectra. However, the addition of ferromagnetic oxides (magnetite) causes strong LB in many natural Al-bearing minerals (Oldfield *et al.*, 1983). If there is an increase in the amount of ferromagnetic compounds associated with the <0.2 μm fraction as a consequence of increased burial history, then this may account for the LB trend observed. A measurement of each sample's bulk magnetic susceptibility would support this idea; unfortunately, this assessment was not available at the time of this study.

An alternate explanation to the increased LB with degree of illitization could be an increase in the paramagnetic LB effectiveness of the Fe. Although there is a clear trend of decreasing Fe content with depth, the Fe that remains associated with the illite structure may cause greater LB than the Fe that is in the smectite sites.

DISCUSSION

Chemical and mineralogical trends in Gulf Coast shales

Having investigated the importance of Fe and the SOQE as potential LB factors that can affect the integrated areas of ^{27}Al NMR spectra, it is now possible to regard the estimates of $^{[4]}Al/^{[4]}Al + {}^{[6]}Al$ ratios as reasonably precise. Measurement of integrated peak areas, using high spinning speeds (<9 KHz) at two different fields, provides equivalent estimates of site populations. The quantitative NMR results of this study are, therefore, in agreement with those of Kinsey *et al.* (1985), Woessner (1989), Morris *et al.* (1990) and Lindgreen *et al.* (1991). Chemical analysis of the I/S portion of the <0.2 μm fraction adjusted by use of Eqs. (1), (4), and (5) are presented in Table 2. Variations in the major chemical components of the I/S phase with depth show trends similar to those observed in other Gulf Coast shales of the same age (Hower *et al.*, 1976). However, for the first time, a quantitative assessment of the Al site distribution within Gulf Coast I/S is presented. Clear trends of decreasing SiO_2, Fe_2O_3 and MgO content with depth are seen accompanying an increase in K_2O with depth. $^{[4]}Al_2O_3$ exhibits a positive increase with depth, while $^{[6]}Al_2O_3$ shows essentially no change at all. These results must first be considered in light of the mineralogical and crystallographic changes that also occur with depth.

Figure 10 illustrates the relative quantitative mineralogy of the <0.2 μm fraction of the shales using the data of Schroeder (1992a). The kaolinite content remains relatively unchanged, which should be noted with regard to the observations of Hower *et al.*, (1976), who show a decrease in kaolinite with depth in the 0.1–0.5 μm fraction. The weight fractions of discrete illite and I/S have a reciprocal relationship with depth (i.e., the ratio of discrete illite to I/S increases with depth). Until this point, it has been assumed, that the initial input of mineralogy of the shales over the range of this study has been relatively uniform. Unfortunately, it is very difficult to track the non-steady state input of the detrital kaolinite and illite, and it is possible that the small variations observed are due to non-steady state

Table 2. Oxide analysis of I/S phase in the <0.2 μm fraction of Miocene shale cuttings from Terrebonne Parish, Louisiana, as determined from electron microprobe, XRD, and ^{27}Al NMR data.

Sample	1220 m	1577 m	2568 m	2779 m	3172 m	3483 m	3758 m	4178 m	4361 m	4673 m	5093 m	5368 m	5764 m
SiO_2	50.68	51.27	50.05	50.11	49.59	49.95	48.22	49.77	47.91	46.47	47.80	47.06	46.93
$^{[4]}Al_2O_3$	4.50	4.80	5.61	4.48	5.25	4.61	5.61	5.16	5.90	6.24	7.49	6.57	7.12
$^{[6]}Al_2O_3$	15.45	15.04	16.05	17.19	16.80	17.10	16.18	16.39	16.26	15.75	17.01	15.09	15.40
Fe_2O_3	8.01	8.54	7.82	5.79	6.61	7.08	6.46	6.31	7.06	6.66	6.13	6.45	5.31
MgO	3.53	3.88	3.44	3.54	3.09	3.21	2.89	3.32	3.03	2.92	3.17	2.56	2.79
Na_2O	1.31	1.11	1.10	1.18	1.25	1.26	1.43	1.57	1.43	1.85	0.92	2.87	1.91
K_2O	1.85	2.52	2.89	2.10	1.79	2.52	2.54	2.85	2.99	2.89	3.26	2.83	3.06

Estimates of precision error average about ±3% of the reported value for each oxide, except Na_2O, which averaged about ±10%.

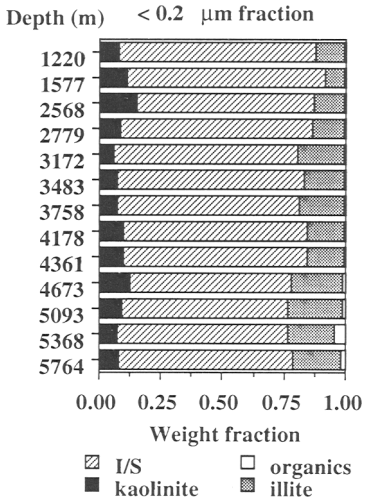

Figure 10. Semiquantitative phase analysis of <0.2 μm fraction of each interval of Miocene Gulf Coast shale studied. Clay mineralogy determined by XRD. Organic content was independently determined by analysis of ashed (450°C) and unashed sample material using an ERBA®C,N analyzer.

effects. The question remains as to whether the small increase in discrete illite is a result of non-steady state input of detrital illite or the addition of newly precipitated illite.

An increase in discrete illite content with depth due to the formation of neoformed illite adds uncertainty to the assumption of constant discrete illite composition. If the composition of detrital discrete illite is different from that of authigenic discrete illite, then the apportionment of chemical components in Table 2 would change. For example, if authigenic discrete illite was forming with a more $^{[6]}$Al-rich, and Fe,Mg-poor composition, then the $^{[6]}Al_2O_3$ trend in the I/S phase should decrease with depth. Given the ^{27}Al NMR constrained chemical data alone, it is not possible to make the distinction between detrital and authigenic discrete illite. Regardless of the assumption about the composition of the discrete illites, it is apparent that major redistributions of structural components are occurring.

Using the general trends in Table 2, the relative gains and losses of the I/S fraction are shown in Table 3. Charge balance considerations of all the cations shown in Table 3 reveal a net negative charge imbalance (i.e., more positive charge lost than gained). Boles and Franks (1979) have shown considerable amounts of hydroxyl and oxygen ion must be released to balance the elementary illitization reaction (Reaction 2 of Boles and Franks). The overall illitization reaction likely involves several phases including feldspars, quartz, organic matter, kaolinite, and chlorite. It is beyond the scope of this paper to address the nature of the overall reaction; however, the evaluation of atomic gains and losses from the I/S phase does serve to evaluate I/S crystal-

Table 3. Oxide wt. % changes and atomic changes (relative to K) in the I/S portion of the <0.2 μm fraction of Miocene shales from 1220 m to 5764 m in depth.

	Estimated change in wt. %	Number of atoms relative to K
SiO_2	−4.0 (±0.4)	−2.4
$^{[4]}Al_2O_3$	+3.0 (±0.3)	+2.1
$^{[6]}Al_2O_3$	0.0 (±0.1)	0.0
Fe_2O_3	−2.5 (±0.3)	−1.1
MgO	−0.8 (±0.1)	−0.7
K_2O	+1.2 (±0.1)	+1.0

Note: The errors associated with estimating the wt. % change are about ±10%; therefore, the numbers of atoms are only approximate values.

chemistry. The change in weight percent for SiO_2 and $^{[4]}Al_2O_3$ (−4.0 and +3.0, respectively) translates to a relative change of about one Si atom for each $^{[4]}$Al atom. Perplexing is the fact that only half the number of K atoms are gained for the charge imbalance created by Si gain and Al loss, particularly in light of new evidence for the formation of a high-charge illite type layer ($K_{0.89}Al_{1.85}Fe_{0.05}Mg_{0.10}Si_{3.20}Al_{0.80}O_{10}$ $(OH)_2$) during burial diagenesis (Schroeder, 1992b; Środoń *et al.*, 1992).

CONCLUSIONS

Quantitative investigation of Miocene Gulf Coast shales and reference clays using ^{27}Al NMR, XRD, and electron microprobe analysis has provided new constraints for the redistribution of major elemental components and crystallographic changes in I/S phases during burial diagenesis. Based upon atomic gains and losses of the I/S phase, it is apparent that major redistributions of structural components are occurring. However, even given additional quantitative NMR constraints on chemical data, it is not possible to make the distinction between detrital and authigenic discrete illite in the <0.2 μm fraction. This later issue continues to keep the true crystal-chemical nature of diagenetic I/S elusive.

The following additional key points have been addressed in this study:

1) The presence of isomorphous Fe^{3+}, substituted for octahedral Al^{3+} in reference micas and clays, results in about a 10% loss of ^{27}Al NMR signal for each 1% increase in Fe_2O_3 content.

2) A comparison of observed and theoretical relationships between ^{27}Al NMR signal intensity and the fraction of dioctahedral Fe^{3+} sites occupied in a range of K-interlayered 2:1 phyllosilicates suggests that octahedral Fe and Al exists in segregated domains in mixed-layer illite/smectites.

3) Most of the line broadening seen in both $^{[4]}$Al and $^{[6]}$Al peaks of I/S from Gulf Coast shales can be attributed to SOQE. The SOQE for the $^{[6]}$Al site in the I/S fraction of shales decreases very slightly with in-

https://doi.org/10.1346/CCMN.1993.0410605 Published online by Cambridge University Press

creasing depth and percent of illite in the I/S, though not enough to effect site quantification. This trend indicates that the electric field gradients about [6]Al sites of the deeper samples are somewhat less distorted than the shallower samples. This is consistent with the establishment of regular ordering I/S layers and greater symmetry of the [6]Al environment within the crystal structure.

4) Quantitative apportionment of cations into the I/S phase of samples from the Gulf Coast diagenetic environment show directly a trend of increasing number of [4]Al sites and no change in the number of [6]Al sites with increasing percent of illite in I/S. Stoichiometry indicates an approximate 1:1 substitution of tetrahedral Al for Si over the 40–68% range of illite in I/S examined.

5) A slight increase in the amount of discrete illite and decrease in I/S is seen with depth. Distinguishing between non-steady state input of detrital illite and the formation of authigenic illite cannot be accomplished by NMR, XRD, and chemical analyses alone. If there are significant compositional differences between these two potential types of discrete illite phases, then the approach for isolation of I/S chemistry must be assessed with caution.

ACKNOWLEDGMENTS

Financial support was provided by a grant-in-aid from Texaco Exploration and Production Technology Division, Houston, Texas. Support was also given by Robert A. Berner at Yale University. The Gulf Coast samples were supplied by Andy Thomas at Texaco. Kurt Zilm of the Yale Chemistry Department is acknowledged for his assistance with the NMR spectroscopy; however, the author takes full responsibility for the interpretation of the data presented. Jim Kirkpatrick at the University of Illinois kindly provided the high field NMR analysis. The author benefited from discussions with Bob Berner, Jim Duchamp, Jim Howard, Ellery Ingall, Tony Lasaga, Bob Reynolds, and Kurt Zilm. The editorial assistance of Stephen Altaner, Ray Ferrell, and Jan Środoń is greatly appreciated.

REFERENCES

Ahn, J. H. and Buseck, P. R. (1990) Layer-stacking sequences and structural disorder in mixed-layer illite/smectite: Image simulations and HRTEM imaging: *Amer. Mineral.* **75,** 267–275.

Alemany, L. B., Massiot, D., Sheriff, B. L., Smith, M. E., and Taulelle, F. (1991) Observation and accurate quantification of ^{27}Al MAS NMR spectra of some Al_2SiO_5 polymorphs containing sites with large quadrupole interactions: *Chem. Phys. Lett.* **177,** 301–314.

Altaner, S. P., Weiss, C. A., and Kirkpatrick, R. J. (1988) Evidence from 29-Si NMR for the structure of mixed-layer illite/smectite clay minerals: *Nature* **331,** 699–702.

Behrens, H. J. and Schnabel, B. (1982) The second order influence of the nuclear quadrupole interaction on the central line in the NMR of quadrupolar nuclei using rapid ample spinning: *Physica* **114B,** 185–190.

Bethke, C. M. and Altaner, S. P. (1986) Layer-by-layer mechanism of smectite illitization and application to a new rate law: *Clays & Clay Minerals* **34,** 136–145.

Boles, J. R. and Franks, S. G. (1979) Clay diagenesis in Wilcox sandstones of southwest Texas. Implications of smectite diagenesis on sandstone cementation: *J. of Sed. Petrology* **49,** 55–70.

Eberl, D. D. and Środoń, J. (1988) Ostwald ripening and interparticle diffraction effects for illite crystals: *Amer. Mineral.* **73,** 1335–1345.

Eberl, D. D., Środoń, J., Lee, M., Nadeau, P. H., and Northrop, H. R. (1987) Sericite form of the Silverton caldera, Colorado: Correlation among structure, composition, origin, and particle thickness: *Amer. Mineral.* **72,** 914–934.

Elliott, W. C., Aronson, J. J., Matisoff, G., and Gautier, D. L. (1991) Kinetics of the smectite to illite transformation in the Denver Basin: Clay mineral, K-Ar data, and mathematical model results: *A.A.P.G. Bulletin* **75,** 436–478.

Fenzke, D., Freude, D., Frohlich, T., and Haase, J. (1981) NMR intensity measurements of half-integer quadrupole nuclei: *Chem. Phys. Lett.* **111,** 171–175.

Ganapathy, S., Schrame, S., and Oldfield, E. (1982) Variable-angle sample-spinning high resolution NMR of solids.: *J. Chem. Phys.* **77,** 4360–4365.

Ghose, S. and Tsang, T. (1973) Structural dependence of quadrupole coupling constant e2qQ/h for 27-Al and crystal field parameter D for Fe^{3+} in aluminosilicates: *Amer. Mineral.* **58,** 748–755.

Giese, R. F. (1988) Kaolin minerals: Structures and stabilities: in *Hydrous Phyllosilicates (Exclusive of Micas), Vol. 19,* S. W. Bailey, ed., Mineralogical Society of America, Washington, D.C., 29–66.

Goodman, B. A. and Stucki, J. W. (1984) The use of nuclear magnetic resonance (NMR) for the determination of tetrahedral aluminium in montmorillonite. *Clay Miner.* **19,** 663–667.

Herrero, C. P. (1987) Monte carlo simulation and calculation of electrostatic energies in the analysis of Si-Al distributions in micas: *Proceedings of the International Clay Conference, Denver,* L. G. Schultz, H. van Olphen, and F. A. Mumpton, eds., The Clay Minerals Society, Denver, 24–30.

Herrero, C. P., Gregorkiewitz, M., and Serratosa, J. M. (1987) 29-Si MAS-NMR spectroscopy of mica type silicates: Observed and predicted distribution of tetrahedral Al-Si: *Phys. Chem. Minerals* **15,** 84–90.

Herrero, C. P., Sanz, J., and Serratosa, M. (1985a) Si, Al distribution in micas: Analysis by high-resolution 29-Si NMR spectroscopy: *J. Phys. C: Solid State Phys.* **18,** 2–22.

Herrero, C. P., Sanz, J., and Serratosa, M. (1985b) Tetrahedral cation ordering in layer silicates by 29-Si NMR spectroscopy: *Solid State Comm.* **53,** 151–154.

Howard, J. J. (1987) Influence of shale fabric on illite/smectite diagenesis in the Oligocene Frio Formation, south Texas: *Proceedings of the International Clay Conference,* L. G. Schultz, H. van Olphen, and F. A. Mumpton, eds., The Clay Minerals Society, Denver, 144–150.

Hower, J., Elsinger, E. V., Hower, M. E., and Perry, E. A. (1976) Mechanism of burial metamorphism of argillaceous sediment: 1. Mineralogical and chemical evidence: *Geol. Soc. Am. Bulletin* **87,** 725–737.

Inoue, A., Kohyama, N., Kitagawa, R., and Watanabe, T. (1987) Chemical and morphological evidence for the conversion of smectite to illite: *Clays & Clay Minerals* **35,** 111–120.

Jakobsen, H. J., Jacobsen, H., and Lindgreen, H. (1988) Solid state 27-Al and 29-Si N.M.R. studies on diagenesis

of mixed layer silicates in oil source rocks: *Fuel* **67,** 727–370.

Kinsey, R. A., Kirkpatrick, R. J., Hower, J., Smith, K. A., and Oldfield, E. (1985) High resolution aluminum-27 and silicon-29 nuclear magnetic resonance spectroscopic study of layer silicates, including clay minerals: *Amer. Mineral.* **70,** 537–548.

Kirkpatrick, R. J. (1988) MAS NMR spectroscopy of minerals and glasses: in *Spectroscopic Methods in Mineralogy and Geology, Vol. 18,* F. C. Hawthorne, ed., Mineralogical Society of America, Washington, D. C., 341–404.

Kirkpatrick, R. J., Oestrike Jr., R., Weiss, C. A., Smith, K. A., and Oldfield, E. (1986) High-resolution 27-Al and 29-Si NMR spectroscopy of glasses and crystals along the join $CaMgSi_2O_6$-$CaAl_2SiO_6$: *Amer. Mineral.* **71,** 705–711.

Lanson, B. and Champion, D. (1991) The I/S to illite reaction in the late stage diagenesis: *Amer. J. Sci.* **291,** 473–506.

Lindgreen, H., Jacobsen, H., and Jakobsen, H. J. (1991) Diagenetic structural transformations in North Sea Jurassic illite/smectite: *Clays & Clay Minerals* **39,** 54–69.

Lippmaa, E., Samoson, A., and Magi, M. (1986) High-resolution 27-Al NMR of aluminosilicates: *J. Am. Chem. Soc.* **108,** 1730–1735.

Massiot, D., Bessada, C., Courures, J. P., and Taulelle, F. (1990) A quantitative study of ^{27}Al MAS NMR in YAG: *J. of Magnetic Resonance* **90,** 231–242.

Milliken, K. L. (1989) Petrography and composition of authigenic feldspars, Oligocene Frio Formation, South Texas: *J. Sed. Petrology* **59,** 361–374.

Moore, D. E. and Reynolds, R. C. (1989) *X-ray Diffraction and the Identification and Analysis of Clay Minerals:* Oxford University Press, New York, p. 332.

Morris, H. D., Bank, S., and Ellis, P. D. (1990) 27-Al NMR spectroscopy of iron-bearing montmorillonite clays: *J. Phys. Chem.* **94,** 3121–3129.

Nadeau, P. H., Wilson, M. J., McHardy, W. J., and Tait, J. M. (1984a) Interstratified XRD characteristics of physical mixtures of elementary clay particles: *Clay Miner.* **19,** 67–76.

Nadeau, P. H., Wilson, M. J., McHardy, W. J., and Tait, J. M. (1984b) Interparticle diffraction: A new concept for interstratified clays. *Clay Miner.* **19,** 757–769.

Nadeau, P. H., Wilson, M. J., McHardy, W. J., and Tait, J. M. (1984c) Interstratified clays as fundamental particles: *Science* **225,** 923–925.

Newman, A. C. D. and Brown, G. (1987) The chemical constitution of clays: in *Chemistry of Clays and Clay Minerals,* A. C. D. Newman, ed., John Wiley & Sons, New York, 1–128.

Oldfield, E., Kinsey, R. A., Smith, K. A., Nichols, J. A., and Kirkpatrick, R. J. (1983) High-resolution NMR of inorganic solids. Influence of magnetic centers on magic-angle sample-spinning line shapes in some natural aluminosilicates: *J. Mag. Resonance* **51,** 325–329.

Pollastro, R. M. (1985) Mineralogical and morphological evidence for the formation of illite at the expense of illite/smectite: *Clays & Clay Minerals* **33,** 265–274.

Samoson, A. (1985) Satellite transition high-resolution NMR of quadrupole nuclei in powders: *Chem. Phys. Lett.* **119,** 29–32.

Sanz, J. and Serratosa, J. M. (1984) 29-Si and 27-Al high-resolution MAS-NMR spectra of phyllosilicates: *J. Am. Chem. Soc.* **106,** 4790–4793.

Schroeder, P. A. (1990) Far-infrared, X-ray diffraction and chemical investigation of potassium micas: *Amer. Mineral.* **75,** 983–991.

Schroeder, P. A. (1992a) Far-infrared study of the interlayer torsional-vibrational mode of mixed-layer illite/smectites: *Clays & Clay Minerals* **40,** 81–91.

Schroder, P. A. (1992b) A multiple reaction mechanism (MRM) model for illitization during burial diagenesis: *29th International Geological Congress, Kyoto, Japan, 29th IGC Workshop* **WB-1,** 79–88.

Środoń, J., McHardy, F. E. W. J., and Morgan, D. J. (1992) Chemistry of illite-smectite inferred from TEM measurements of fundamental particles: *Clay Miner.* **27,** 137–158.

Środoń, J., Morgan, D. J., Eslinger, E. V., Eberl, D. D., and Karlinger, M. R. (1986) Chemistry of illite/smectite and end-member illite: *Clays & Clay Minerals* **34,** 368–378.

Surdam, R. C. and Crossey, L. J. (1987) Integrated diagenetic modeling: A process-oriented approach for clastic systems: *Ann. Rev. Earth Planet. Sci.* **15,** 141–170.

Taulelle, F., Bessada, C., and Massiot, D. (1992) Quantitative analysis of MAS NMR quadrupole nuclei: *J. de Chimie Physique* **89,** 379–385.

Taylor, R. M. (1980) Non-silicate oxides and hydroxides: in *Crystal Structures of Clay Minerals and Their X-ray Identification,* G. W. Brindley and G. Brown, eds., Mineralogical Society, London, 129–201.

Tellier, K. E., Hulchy, M. M., Walker, J. R., and Reynolds, R. C. (1988) Application of high gradient magnetic separation (HGMS) to structural and compositional studies of clay mineral mixtures: *J. Sed. Petrology* **58,** 761–763.

Whitney, G. and Northrop, H. R. (1988) Experimental investigation of the smectite to illite reaction: Dual reaction mechanism and oxygen-isotope systematics: *Amer. Mineral.* **73,** 77–90.

Woessner, D. E. (1989) Characterization of clay minerals by 27-Al nuclear magnetic resonance spectroscopy: *Amer. Mineral.* **74,** 203–215.

(Received 16 February 1993; accepted 8 July 1993; Ms. 2325)